MOLECULAR BIOLOGY

Loss of PRC1 activity in different stem cell compartments activates a common transcriptional program with cell type–dependent outcomes

Silvia Pivetti[1], Daniel Fernandez-Perez[1], Alessandro D'Ambrosio[1], Caterina Maria Barbieri[1], Daria Manganaro[1], Alessandra Rossi[1], Laura Barnabei[1]*, Marika Zanotti[1], Andrea Scelfo[1], Fulvio Chiacchiera[1,2†‡], Diego Pasini[1,3†‡]

Polycomb repressive complexes are evolutionarily conserved complexes that maintain transcriptional repression during development and differentiation to establish and preserve cell identity. We recently described the fundamental role of PRC1 in preserving intestinal stem cell identity through the inhibition of non–lineage-specific transcription factors. To further elucidate the role of PRC1 in adult stem cell maintenance, we now investigated its role in LGR5+ hair follicle stem cells during regeneration. We show that PRC1 depletion severely affects hair regeneration and, different from intestinal stem cells, derepression of its targets induces the ectopic activation of an epidermal-specific program. Our data support a general role of PRC1 in preserving stem cell identity that is shared between different compartments. However, the final outcome of the ectopic activation of non–lineage-specific transcription factors observed upon loss of PRC1 is largely context-dependent and likely related to the transcription factors repertoire and specific epigenetic landscape of different cellular compartments.

INTRODUCTION

Cellular identity is preserved by different layers of transcriptional control. Among the factors and molecular circuits involved in establishing and maintaining cell type–specific transcriptional profiles, epigenetic regulators play a pivotal role. Alterations in these mechanisms are one of the leading causes of different pathologies, such as cancer (*1*, *2*). Polycomb group (PcG) proteins are a class of evolutionarily conserved molecules required to maintain transcriptional repression during development and differentiation (*3*). PcG proteins assemble into two major complexes named Polycomb repressive complex 2 (PRC2) and PRC1. PRC1 and PRC2 share the vast majority of their targets, characterized by CpG-rich regions at promoters, where they are recruited sequentially. The core of PRC2 is composed of the mutually exclusive catalytic subunits EZH1 and EZH2, which deposit the mono-, di-, and trimethylation on lysine 27 of histone H3 (H3K27me3), and of two structural proteins SUZ12 and EED, which are necessary for complex formation and stabilization (*4*, *5*). PRC1 is responsible for the deposition of a single ubiquitin moiety on lysine 119 of histone H2A (H2AK119Ub1) through the catalytic subunits RING1A or RING1B. In addition, it has been described that PRC1 exists in several different forms characterized by the presence of different mutually exclusive Polycomb group ring finger (PCGF) proteins (*6*). These different complexes have been defined as "canonical" or "noncanonical" depending on their ability to associate with chromobox (CBX) proteins. While CBX-containing canonical PRC1 complexes are tethered to chromatin by PRC2-dependent deposition of H3K27me3, the recruitment of noncanonical complexes remains independent of PRC2 activity.

The activity and biological function of PRC1 and PRC2 has been intensively investigated in the past 20 years during embryonic development and using embryonic stem cells (ESCs) (*3*, *5*), while their role in adult stem cells and tissue homeostasis has only recently attracted attention (*7*–*14*). Adult tissues are constantly regenerated and maintained by a pool of stem cells, which are able to compensate for cell loss and tissue damage while preserving stem cell pools (*15*). We recently uncovered the central role of PRC1 activity in preserving intestinal stem cell (ISC) identity through the transcriptional repression of non–lineage-specific transcription factors (TFs), which are able to interfere with the transcriptional program stimulated by the Wnt pathway required for the maintenance of the ISC pool (*9*). With the aim to uncover whether this is a general PcG role in adult stem cells, we now investigated the consequences of PRC1 loss of activity in a stem cell compartment from a different tissue with a distinct developmental origin—hair follicle stem cells (HFSCs).

The skin is the largest organ of the body. It is the first barrier against external insults such as bacteria and virus infections, toxic agents, and ultraviolet radiation, preserving, at the same time, water and temperature homeostasis. In mammals, the epidermis comprises the interfollicular epidermis and the pilosebaceous unit composed of the hair follicle (HF) and the sebaceous gland. During morphogenesis, which begins after delivery, HFs grow downward in the dermal compartment of the skin from the hair bulge and its associated germ (*16*). Hair regeneration is fueled by two different stem cell pools located in the bulge and hair germ. The bulge contains both CD34+ and LGR5+ (Leucine Rich Repeat Containing G Protein-coupled-receptor-5) stem cells, while the hair germ is exclusively colonized by LGR5+ stem cells (*17*, *18*). Throughout life, HFs cycle between proliferation (anagen), destruction (catagen), and resting (telogen) phases (*19*). Anagen onset is activated when WNT proliferative signals overcome a bone morphogenetic protein threshold (*20*, *21*), and LGR5+ HFSCs are essential during anagen to sustain HF growth (*22*). These cells first proliferate to form multipotent progenitors that briefly divide and give rise to matrix cells that will generate all the inner layers of the differentiating

[1]European Institute of Oncology–IRCCS, Department of Experimental Oncology, Milan, Italy. [2]University of Trento, Department of Cellular, Computational and Integrative Biology–CIBIO, Trento, Italy. [3]University of Milan, Department of Health Sciences, Milan, Italy.
*Present address: Imagine Institute, Paris, France.
†These authors contributed equally to this work.
‡Corresponding author. Email: fulvio.chiacchiera@unitn.it (F.C.); diego.pasini@ieo.it (D.P.)

HF (23, 24). During anagen progression, LGR5$^+$ stem cells expand downward to constitute the outer root sheet (ORS) that delimitates the follicle. During anagen phase, LGR5$^+$ HFSCs appear to be functionally similar to LGR5$^+$ ISCs, being actively proliferating stem cells supporting a renewing tissue. For these reasons, they represent a good system to uncover general, stem cell–specific PRC1 activities.

Here, we report that the activity of PRC1 is essential to sustain LGR5$^+$ HFSC and general HF regeneration. We further characterized the direct molecular circuits triggered by PRC1 loss of function and found that, despite the fact that a large part of PRC1 activity is associated with active gene expression, the phenotypic outcome of its loss of function can be primarily ascribed to its canonical repressive functions. In this context, PRC1 is directly involved in suppressing an epidermal transcriptional program maintaining silencing of the master epidermal regulator *Ascl2*. Taking advantage of parallel data generated in ISCs, we further show that, despite the fact that PRC1 retains a general role in suppressing developmental programs across tissue and stem cell compartments, the molecular phenotypes triggered by PRC1 loss of function are strongly dependent on the cellular context, and therefore, by the repertoire of the expressed TFs in any given cell.

RESULTS

PRC1-dependent H2AK119Ub1 is required for HF regeneration

To uncover the general mechanisms by which PRC1 activity contributes to lineage identity in different adult stem cell populations, we took advantage of the *LGR5-GFP-ires-CreERT2/Ring1a$^{-/-}$/Ring1b$^{fl/fl}$/Rosa26lox-stop-lox LacZ* compound model (hereof *Ring1a/b* ctrl or dKO upon tamoxifen treatment) that we have previously generated (fig. S1A) (9). The *Lgr5* transgene is homogenously expressed in a population of actively cycling and long-lived HFSCs that, from the base of the hair bulb, gradually expand through the ORS, contributing to the regeneration of the follicle (18). We used this genetic model to acutely abrogate PRC1 activity in 8 to 12 weeks, sex-matched mice and showed that four daily tamoxifen injections are sufficient to abolish PRC1 activity in LGR5$^+$ [green fluorescent protein–positive (GFP$^+$)] HFSCs, as shown by the loss of H2AK119Ub1 in GFP$^+$ cells of telogen HFs (Fig. 1, A and B).

HF regeneration in adult mice is a critical mechanism through which fur is maintained during the entire life span. HFs cycle synchronously during the first 10 to 11 weeks of age and then gradually loose synchrony, despite maintaining the same regenerating capabilities (fig. S1B) (18, 19, 25). To investigate the role of PRC1 in adult HFSCs during HF regeneration, we exploited the possibility to resynchronize HFs by means of follicles plucking. As soon as the hair is removed, follicles rapidly and synchronously enter into anagen phase and start to cycle (25). To abrogate PRC1 activity from the first phases of HF regeneration, we administered tamoxifen in adult mice 1 day before waxing the back skin (Fig. 1C). After 12 days from waxing, while the fur of *Ring1a/b* ctrl mice was completely regenerated (Fig. 1D, top), we severely delayed follicle regeneration in *Ring1a/b* dKO mice in the absence of PRC1 activity (Fig. 1D, bottom). We further confirmed this result by lineage-tracing analyses, taking advantage of a *Rosa26lox-stop-lox LacZ* allele to follow LACZ expression in the progeny of LGR5$^+$ stem cells. Twelve days after waxing, we markedly reduced the number of β-galactosidase (β-Gal)–expressing HFs in *Ring1a/b* dKO animals, suggesting that the residual hair growth is derived from wild-type HFs (Fig. 1E).

PRC1 depletion affects the onset of anagen phase and the HF cycle

To elucidate whether PRC1 activity is required for entering into or to progress through the anagen phase, we activated Cre-mediated recombination at P49 to induce Ring1b loss of function during the long telogen period. After 2 weeks from tamoxifen exposure, we synchronized HFs by waxing and then collected the back skin after 8 and 12 days (Fig. 2A and fig. S2A) to perform histological analyses and β-Gal staining to trace PRC1-null progeny. After 8 days from waxing, we observed a substantial delay in hair growth in *Ring1a/b* dKO mice (fig. S2B). This was further confirmed by histological analysis showing shorter HFs, blocked in the early anagen phases (I and II) [fig. S2, C (top) and D] (25). At 8 days from waxing, the total number β-Gal$^+$ HFs was strongly reduced in *Ring1a/b* dKOs [fig. S2, C (bottom) and E]. It is well established that the hypodermal adipocyte layer fluctuates in thickness during the hair cycle (25, 26). This increases during anagen and reduces throughout catagen to reach a resting phase until a new hair cycle begins. *Ring1a/b* dKOs displayed a clear imbalance of hypodermis fat (fig. S2F) and dermis thickness (fig. S2G), despite the fact that the total skin showed a similar width (fig. S2H). This reinforces evidence that PRC1 loss severely affects HF regeneration. This phenotype was confirmed and enhanced after 12 days from waxing (Fig. 2B). According to Müller-Röver *et al.* (25) classification, at this time point, while *Ring1a/b* ctrl mice showed all features of full anagen (anagen phase VI), *Ring1a/b* dKO follicles still resembled primary stages of the hair cycle (anagen phases II and III; Fig. 2C, top). Lineage tracing of LGR5$^+$ stem cell progeny showed a marked reduction of cells derived from *Ring1a/b* dKO stem cells, as demonstrated by the severe lack of β-Gal staining compared to ctrl follicles [Fig. 2, C (bottom) and D]. Consistently, the differences in follicles length, hypodermis, and dermis thickness were further increased at 12 versus 8 days after waxing, with a similar reduced number of HFs (Fig. 2, E to H, and fig. S2, I to L). Together, these data suggest that the loss of PRC1 activity does not fully prevent entry into the anagen phase but rather impairs the regenerative potential of LGR5$^+$ stem cells.

Conserved PRC1-repressed transcriptional programs are required to preserve HFSCs and ISCs

Our results suggest that the loss of PRC1 induces similar phenotypic outcomes in HFSCs compared to our previous results with ISCs (9). Whether this involves common or cell type–specific pathways remains an important open question. To investigate the transcriptional changes induced by PRC1 loss of function in anagen-activated LGR5$^+$ stem cells, we collected the skin of *Ring1a/b* dKO and ctrl adult mice 8 days from waxing (Fig. 3A). HFs were isolated and reduced at single cells, and LGR5$^+$ cells were isolated by fluorescence-activated cell sorting (FACS) to perform RNA sequencing (RNA-seq) analyses. FACS analysis on the same cells stained for H2AK119Ub1 demonstrated that tamoxifen treatment results in >70% loss of PRC1 activity in LGR5$^+$ (GFP$^+$) cells (Fig. 3B). RNA-seq analysis in these cell populations revealed a >5-fold bias in genes up-regulation (1066 up-regulated versus 187 down-regulated genes) that is consistent with the general PRC1 role as transcriptional repressor also in the HF compartment (Fig. 3C). Gene ontology (GO) analysis on differentially expressed genes showed that up-regulated genes are primarily associated with general developmental processes (Fig. 3D). In contrast, down-regulated genes were specifically enriched by factors involved in HF morphogenesis, HFSC maintenance, and hair cycle progression (Fig. 3E), such as Sonic hedgehog (23, 27). Moreover,
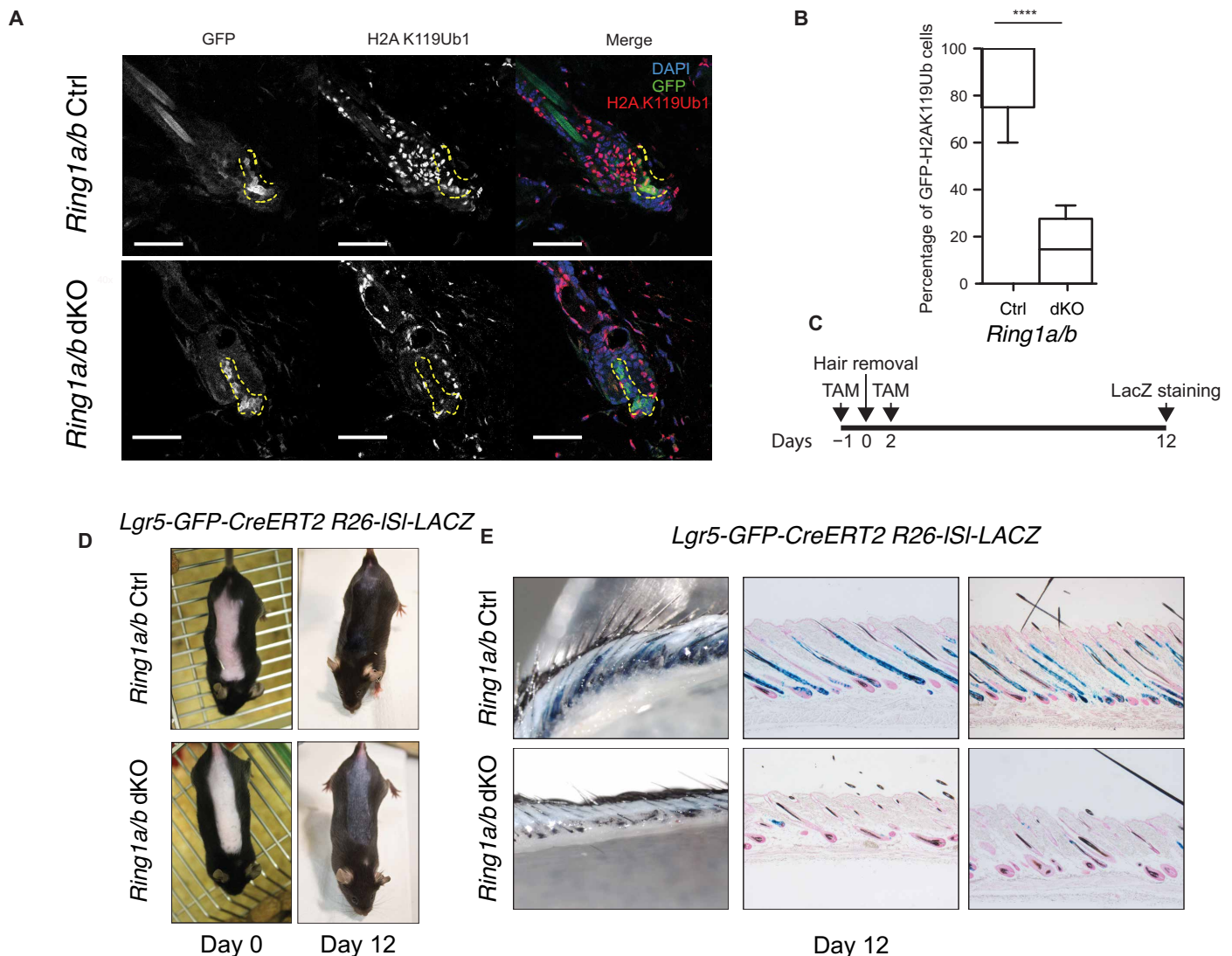
Fig. 1. PRC1 activity is required to sustain HF regeneration. (A) Immunostaining using H2AK119Ub1 (red) and 4′,6-diamidino-2-phenylindole dihydrochloride (DAPI; blue) of HF from LGR5-eGFP-ires-CREERT2 HFSCs in *Ring1a/b*$^{+/+}$ and *Ring1a/b*$^{-/-}$ mice . Scale bars, 50 μm. (Photo credit: F.C. and S.P., European Institute of Oncology). **(B)** Quantification of H2AK119Ub1$^+$ HFSCs in *Ring1a/b*$^{+/+}$ and *Ring1a/b*$^{-/-}$ mice. ****$P < 0.0001$ (P values were calculated with two side t test). TAM, tamoxifen. **(C)** Schematic representation of the protocol used in (D) and (E). **(D)** Representative pictures of *Ring1a/b*$^{+/+}$ and *Ring1a/b*$^{-/-}$ mice immediately after hair removal and after 12 days. (Photo credit: F.C., European Institute of Oncology). **(E)** In vivo lineage tracing of HFSCs. Mice were treated as described in (C), and skin was collected at indicated time point. Samples were stained with X-Gal. Whole tissues were imaged before paraffin embedding, and the sections obtained were counterstained using neutral red. (Photo credit: F.C., European Institute of Oncology).

functional annotation revealed that DNA binding TFs, and particularly homeotic TFs, were overrepresented among the genes upregulated in *Ring1a/b* dKO (fig. S3A). The additional comparison in respect to transcriptional data obtained from several tissues (ENCODE; fig. S3B, bottom) highlighted that the loss of PRC1 activity results in the transcriptional activation of non–lineage-specific genes that are preferentially expressed in distinct tissue compartments. In contrast, down-regulated genes were primarily expressed in activated LGR5$^+$ HFSCs (fig. S3B, top), further corroborating impaired activation of HFSC regenerative capabilities in the absence of PRC1 activity. These data are in agreement with our previous finding in ISCs (*9*), further highlighting the conserved essential role of PRC1 in maintaining lineage identity within adult tissues. Whether this involves

common or specific mechanisms remains an open question. Thus, we searched for common classes of genes that could be potentially involved with the loss of cell identity in ISCs versus HFSCs upon PRC1 inactivation. We compared RNA-seq profiles in both stem cell compartments and found that none of the down-regulated genes were in common in accordance with the distinct identity of the two stem cell populations (fig. S3C). In contrast, we found approximately one-fourth of the up-regulated genes (255 genes, ≈25%) in common between ISC and HFSC (fig. S3D). This group of genes was enriched by mainly homeobox-containing TFs involved in regulating general developmental processes (fig. S3E). Several ZIC (Zinc finger protein of the cerebellum) TFs (*Zic1*, *Zic4*, and *Zic5*; fig. S3F), as well as *Sox7*, *Hoxa10*, and *Hoxb13* (fig. S3G), were present within this list. Together, these data suggest that
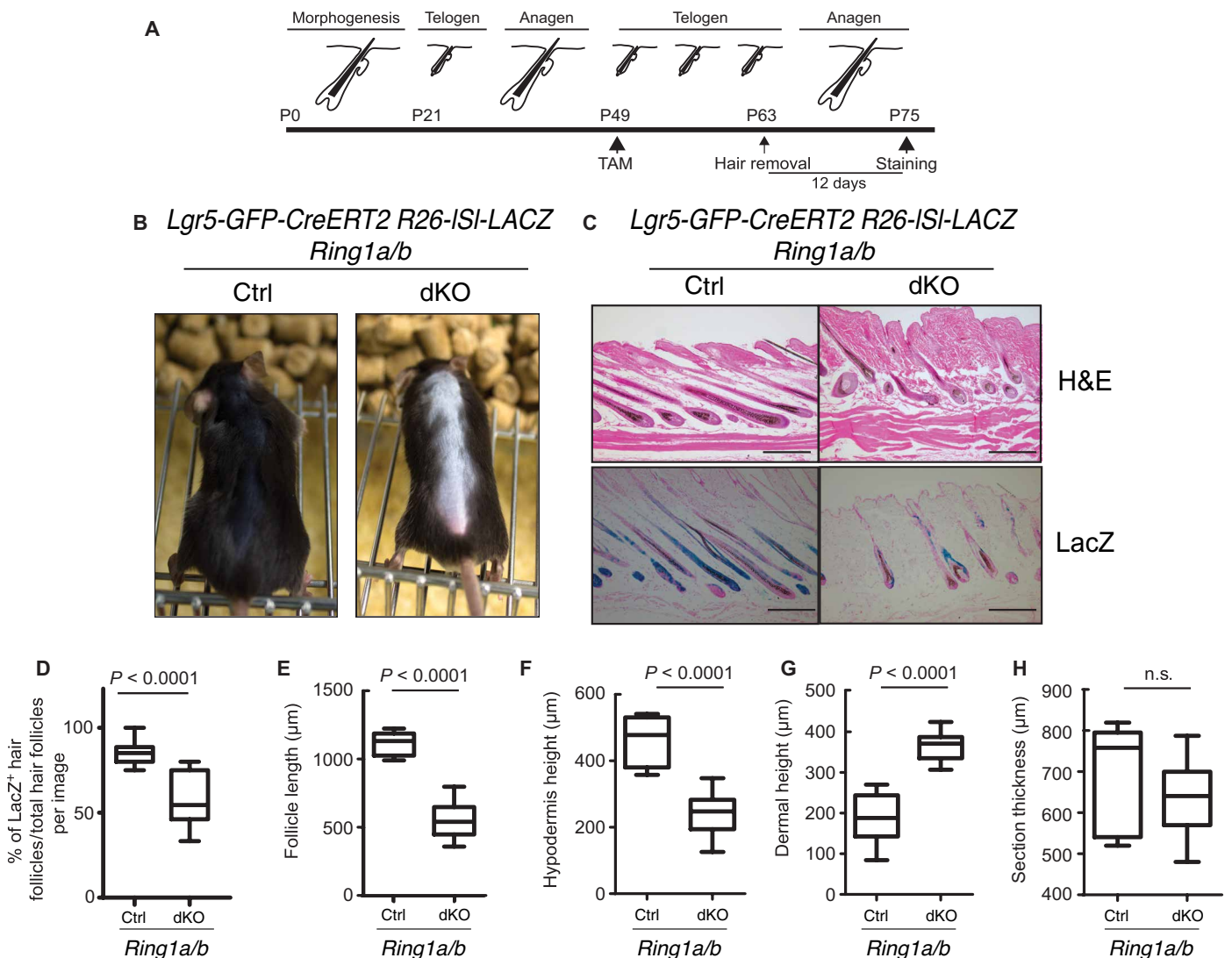
Fig. 2. PRC1 activity is required for anagen onset and progression. (**A**) Schematic representation of the experiment. Tamoxifen was delivered intraperitoneally once a day for four consecutive days during the long telogen phase. At 63 days, postdelivery hairs were removed, and samples were collected after 12 days. (**B**) Representative pictures of *Ring1a/b*[+/+] and *Ring1a/b*[−/−] mice immediately after hair removal and after 12 days. (Photo credit: S.P., European Institute of Oncology). (**C**) Histological analysis and in vivo lineage tracing of HFSCs. Mice were treated as described in (A). Skin was collected at the indicated time points. All collected sample were paraffin-embedded and stained with either X-Gal or hematoxylin and eosin (H&E). Scale bars, 250 μm. (Photo credit: S.P., European Institute of Oncology). (**D**) Quantification of β-Gal[+] HFs, (**E**) HF length, (**F**) hypodermis, (**G**) dermal height, and (**H**) total section thickness at 12 days after waxing in *Ring1a/b*[+/+] and *Ring1a/b*[−/−] mice. All *P* values were calculated with two-side *t* test. n.s., not significant.

PRC1 plays a common general role in distinct stem cell compartments to prevent activation of non–lineage-specific, homeobox-containing TFs.

Transcriptional repression of a subset of canonical PRC1 targets preserves stem cell identity

Recently, two major classes of PRC1 complexes have been described (*6*) on the basis of their biochemical composition. Canonical PRC1, which contains CBX proteins, is recruited on their targets in a PRC2-dependent manner. Noncanonical PRC1 complexes do not contain the CBX-containing subunits and are recruited independently from PRC2. They are characterized by the presence of different PCGF subunits and share the subunits RYBP (RING1 and YY1 Binding Protein) or YAF2 (YY1 Associated Factor 2). Different components of canonical

and noncanonical PRC1 complexes are expressed in HFSCs (fig. S4A). To investigate the ability of RING1B to enter both canonical and non-canonical complexes in HFSCs, we performed proximity ligation assay (PLA). Wild-type and dKO LGR5^{+} HFSCs from waxed mice have been sorted (fig. S4, B and C) and used to investigate the ability of RING1B to interact with RYBP (Fig. 3, F and G) or BMI1 (Fig. 3, H and I). Our data indicate that in HFSCs, both canonical and noncanonical complexes assemble, suggesting that the phenotype observed in dKO HFSCs could be the result of the impaired activity of different complexes.

To identify the common mechanisms through which PRC1 regulates cell fate determination in different stem cell populations, we performed chromatin immunoprecipitation sequencing (ChIP-seq)
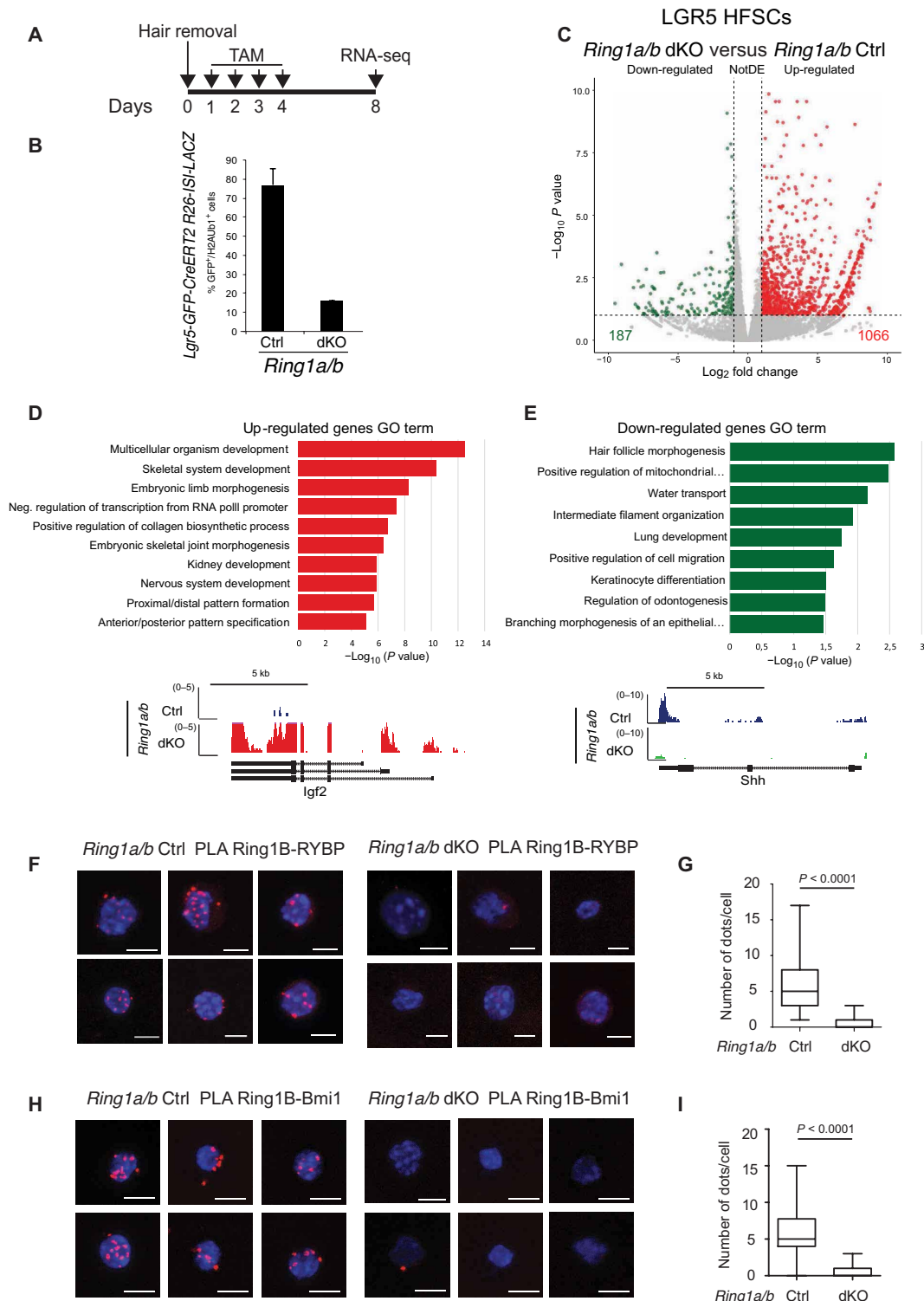
Fig. 3. Loss of PCR1 activity affects HFSCs transcriptional landscape. (**A**) Schematic view of the experiment. (**B**) Quantification of H2AK119Ub1⁺ HFSCs used for RNA-seq experiments in *Ring1a/b*[+/+] and *Ring1a/b*[−/−] mice. HFs were collected 8 days after waxing. Single-cell suspension was stained using anti-H2Ak119Ub1 and analyzed by FACS. (**C**) Volcano plot of differentially expressed genes between *Ring1a/b*[+/+] and *Ring1a/b*[−/−] mice. Log₂ fold change, ≥1. (**D**) GO analysis of up-regulated and (**E**) down-regulated genes in *Ring1a/b*[−/−] mice (log₂ fold change, ≥1) representative snapshots of modulated genes is shown. Shh, Sonic hedgehog. (**F**) PLA between RING1B and RYBP on *Ring1a/b*[+/+] and *Ring1a/b*[−/−] HFSCs. (Photo credit: S.P. and A.D., European Institute of Oncology). (**G**) Quantification of RING1B-RYBP PLA dots per cell in *Ring1a/b*[+/+] and *Ring1a/b*[−/−] HFSCs. (**H**) PLA between RING1B and BMI1 on *Ring1a/b*[+/+] and *Ring1a/b*[−/−] HFSCs. (Photo credit: S.P. and A.D., European Institute of Oncology). (**I**) Quantification of RING1B-BMI1 PLA dots per cell in *Ring1a/b*[+/+] and *Ring1a/b*[−/−] HFSCs. Scale bars, 5 μm. All *P* values were calculated with two-side *t* test.

analysis for RING1B in FACS-sorted activated LGR5^{+} stem cells purified 8 days from waxing (Fig. 4, A and B). This analysis identified nearly 3900 RING1B significant peaks that were mainly associated with promoter regions (Fig. 4C). This distribution closely resembles the RING1B chromatin association that we have found in ISCs (Fig. 4D). Since RING1A or RING1B can form distinct functional complexes that may localize differently along the genome (6), we first compared the genomic localization of RING1B in both HFSCs and ISCs in respect to the deposition of H3K27me3 to define Polycomb-repressed domains (9, 28). We restricted the extent of overlap with the canonical PcG-repressed domains only to 20% of RING1B sites in HFSCs (Fig. 4E) and to 10% in ISCs (Fig. 4F), suggesting that a large fraction of RING1B activity is exerted independently of PRC2. In ESCs, H3K27me3 is enriched at promoters of developmental-related genes concomitantly with the deposition of the transcriptional activatory modification H3K4me3. This promoter status has been defined as "bivalent" or "poised" (29). Bivalency is resolved when ESCs are triggered to differentiate by the acquisition of a purely active (H3K4me3 only) or repressed (H3K27me3 only) state. We found that, while only 30% of H3K27me3 sites in HFSC are bivalent (coenriched with H3K4me3), this proportion expands in ISCs where it reaches 80% of all RING1B target promoters enriched for H3K27me3 (Fig. 4, G and H). We also observed a large fraction of RING1B-bound sites that lacks H3K27me3 but presents H3K4me3 deposition (Fig. 4, I and J). Accordingly, with the ability of RING1B to interact with subunits of both canonical and noncanonical complexes, we observed that in HFSCs, nearly 70% of RYBP peaks colocalize with RING1B (Fig. 4K), but only a small percentage (11%) of the co-occupied regions harbor H2AK119Ub (Fig. 4L). Those regions characterized by the presence of RING1B and H2AK119Ub are also occupied by CBX8, a canonical PRC1 subunit, and are decorated by PRC2-dependent H3K27me3 mark (Fig. 4, M and N). These data suggest that both canonical and noncanonical PRC1 activities, which are not associated with H3K27me3 and H2AK119Ub, could contribute in the maintenance of stem cell identity.

To address this issue, we ranked all RING1B target promoters based on their expression in wild-type cells, and we compared their expression in PRC1-defective HFSCs and ISCs (Fig. 4O and fig. S5A). This analysis identified four classes of genes. Repressed genes in wild-type cells defined cluster 1 and were enriched for transcriptionally activated genes in *Ring1a/b* dKO HFSCs and ISCs. Genes with intermediate expression (clusters 2 and 3) showed no difference (Fig. 4O) or slightly decreased expression (fig. S5A) in *Ring1a/b* dKO cells. Highly expressed genes (cluster 4) were slightly downregulated in *Ring1a/b* dKO HFSC. The distribution of H3K27me3, H2AK119Ub, and H3K4me3 (Fig. 4P and fig. S5B) identified genes belonging to cluster 1 as fully silenced through canonical Polycomb activities, as demonstrated by the presence of CBX8 (Fig. 4P). These sites are devoid of H3K4me3, which is instead enriched at all the other clusters (Fig. 4P and fig. S5B) where colocalizes with RING1B and RYBP (Fig. 4P). Accordingly, genes involved in development and differentiation were only enriched in cluster 1 (Fig. 4Q and fig. S5, C, E, and F). Despite the fact that these data support a prominent role for canonical versus noncanonical activities in maintaining cell identity in HFSCs and ISCs, it is important to stress that only a subset of RING1B^{+}/H3K27me3[+]/H2AK119Ub targets become derepressed upon the loss of PRC1 activity in HFSCs and ISCs (Fig. 4R and fig. S5D). This suggests, first, that H3K27me3 is largely sufficient to

prevent TF accessibility and activation of PcG targets and, second, that only a small proportion of PcG target genes contribute to the observed phenotypes.

Loss of PRC1 activity activates epidermal-specific program
To uncover direct mechanisms associated with PRC1 loss of activity, we focused our attention on RING1B targets that became derepressed in *Ring1a/b* dKO. This includes *Ascl2* (Fig. 5A), which encodes for a TF previously shown to be sufficient and required to drive epidermal differentiation (30). To investigate whether a specific differentiation program is initiated upon PRC1 activity loss, we performed gene set enrichment analysis (GSEA) comparing signatures from different cells belonging to distinct skin compartments (31) against *Ring1a/b* dKO versus ctrl transcriptional outcome in HFSCs. This analysis showed that, together with the stem cell signature, genes involved in epidermal-specific transcriptional program became enriched in *Ring1a/b* dKO mice (Fig. 5B). Among them, *Satb1*, *Krtdap*, *Calm5*, *Itgam*, and *Gdpd2*, together with *Ascl2*, were some of the known epidermal markers that are highly activated (Fig. 5, A, C, and D). We further scanned the *Ascl2* promoter with LASAGNA-Search 2.0 (32) for putative TFs responsible for its activation and found several binding motifs that are recognized by the family of ZIC TFs (Fig. 5E). Note that different members of this TF family are also directly bound and derepressed in *Ring1a/b* dKO HFSCs (fig. S3F), establishing a positive feedback loop driving epidermal identity. Together, these results support a model in which PRC1 directly suppresses an epidermal-specific transcriptional program via suppression of master regulators of lineage specification, thus contributing to preserve HF identity.

DISCUSSION
The role of Polycomb complexes in maintaining adult stem cell identity has been investigated by several groups during the past 5 years. We recently reported that PRC1 and PRC2 play a crucial role in supporting intestinal homeostasis (8–10). Along the crypt-to-villus axis, the balance between secretory cells and enterocytes differentiation, transit-amplifying cell proliferation and stem cell maintenance are preserved by Polycomb complexes. In particular, PRC1 is critically required for ISC maintenance, and the loss of RING1A/B subunits leads to stem cell exhaustion. Its activity is required to maintain repressed non–lineage-specific TFs, some of which are able to interfere with the ISC-specific transcriptional programs. Stem cell loss observed in RING1A/B-deficient intestinal epithelium can therefore be ascribed not to the initiation of a defined transcriptional program but to the loss of stem cell–specific ones. To unveil general mechanisms underlying PRC1-dependent adult stem cell maintenance, we extended its analysis in proliferating HFSCs. Similar to what we previously described for ISCs, the loss of RING1A/B in HFSCs markedly affects HF regeneration. This phenotypic convergence is mirrored at a transcriptional level by the up-regulation of non–lineage-specific genes, enriched for DNA binding TFs. We provide evidence that PRC1 associates at H3K27Me3[+] promoters of repressed genes in the context of canonical complexes, characterized by the presence of CBX8 subunit and H2AK119Ub. At promoters of active genes, RING1B occupancy coincides with RYBP and low or undetectable H2AK119Ub levels, suggesting that noncanonical PRC1 complexes could play a role at these promoters that is largely independent from their ability to modify histone H2A. A similar
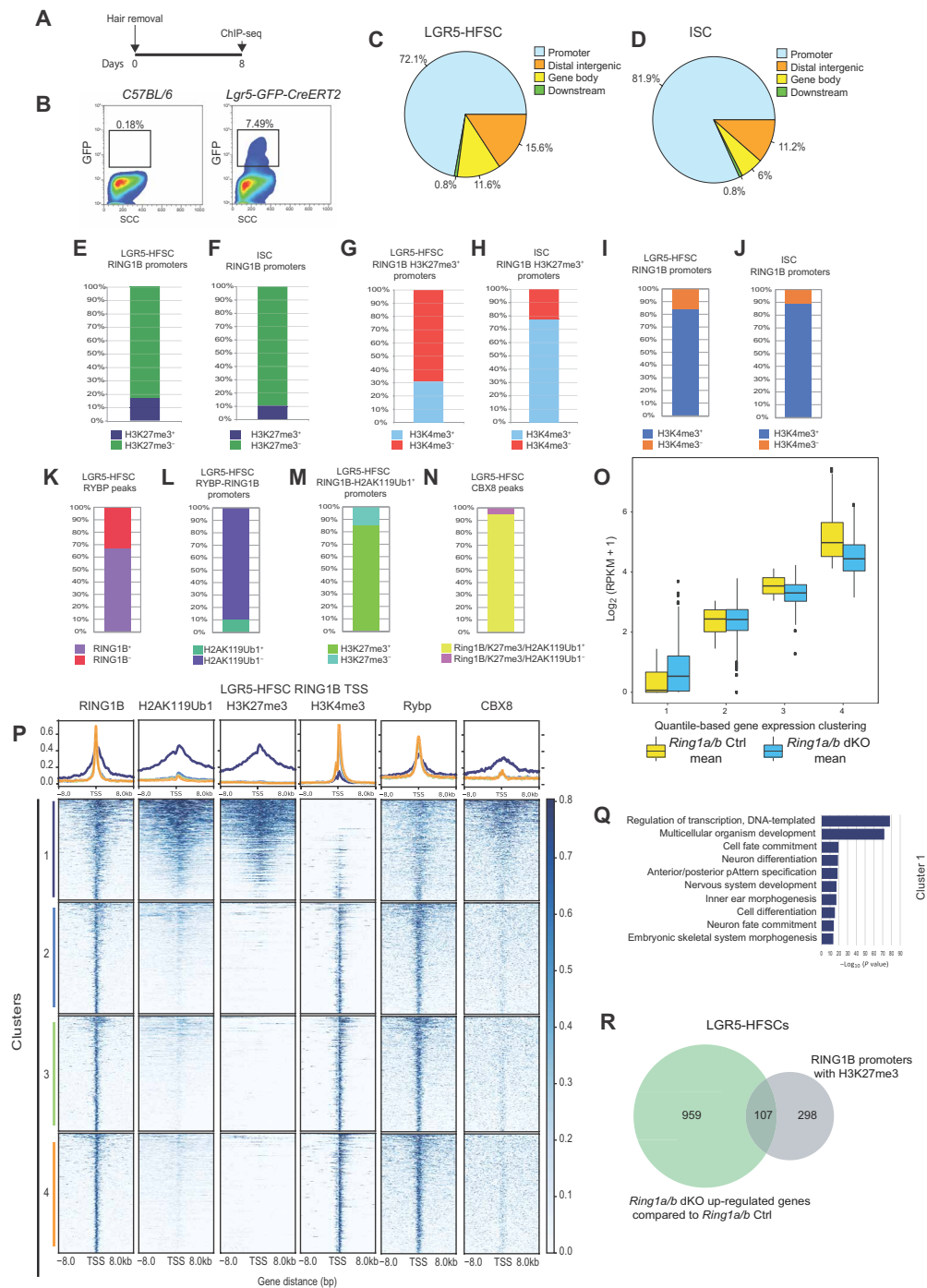
Fig. 4. Genomic distribution of PRC1 binding in HFSCs and ISCs. (**A**) Schematic view of ChIP-seq experiment. (**B**) Gating strategy used to sort HFSCs used in ChIP-seq experiments. (**C**) Genomic distribution of RING1B-bound sites in LGR5^{+} HFSCs. (**D**) Genomic distribution of RING1B-bound sites in LGR5^{+} ISCs. (**E**) Bar plots showing the fraction of RING1B-bound promoters marked by H3K27me3 in HFSCs. (**F**) Bar plots showing the fraction of RING1B-bound promoters marked by H3K27me3 in ISCs. (**G**) Bar plots showing the fraction of RING1B-bound H3K27Me3[+] promoters marked by H3K4Me3 in HFSCs. (**H**) Bar plots showing the fraction of RING1B-bound H3K27Me3[+] promoters marked by H3K4me3 in ISCs. (**I**) Bar plots showing the fraction of RING1B-bound promoters marked by H3K4me3 in HFSCs. (**J**) Bar plots showing the fraction of RING1B-bound promoters marked by H3K4me3 in ISCs. (**K**) Bar plot showing the fraction of RYBP peaks overlapping with RING1B peaks in HFSCs. (**L**) Bar plot representing the percentage of promoters occupied by RYBP and RING1B marked by H2AK119Ub1 in HFSCs. (**M**) Bar plot showing the percentage of promoters occupied by RING1B and H2AK119Ub marked by H3K27Me3 in HFSCs. (**N**) Bar plot showing the percentage of CBX8 peaks overlapping with RING1B, H3K27Me3, and H2AK119Ub triple-positive peaks in HFSCs. (**O**) Quantile-based gene expression clustering performed using $Ring1a/b^{+/+}$ RNA-seq data, showing expression variations between $Ring1a/b^{+/+}$ and $Ring1a/b^{-/-}$ HFSCs. (**P**) Heatmap representing normalized RING1B, H3K27me3, H3K4Me3, H2AK119Ub1, CBX8, and RYBP ChIP-seq intensities of ±8 kb from TSS of RING1B target genes in HFSCs. Clusters were made according to Fig. 4O. bp, base pair. (**Q**) GO analyses of genes belonging to cluster 1. (**R**) Venn diagram showing the overlap between up-regulated genes in $Ring1a/b^{-/-}$ mice with total RING1B/H3K27me3-enriched regions.
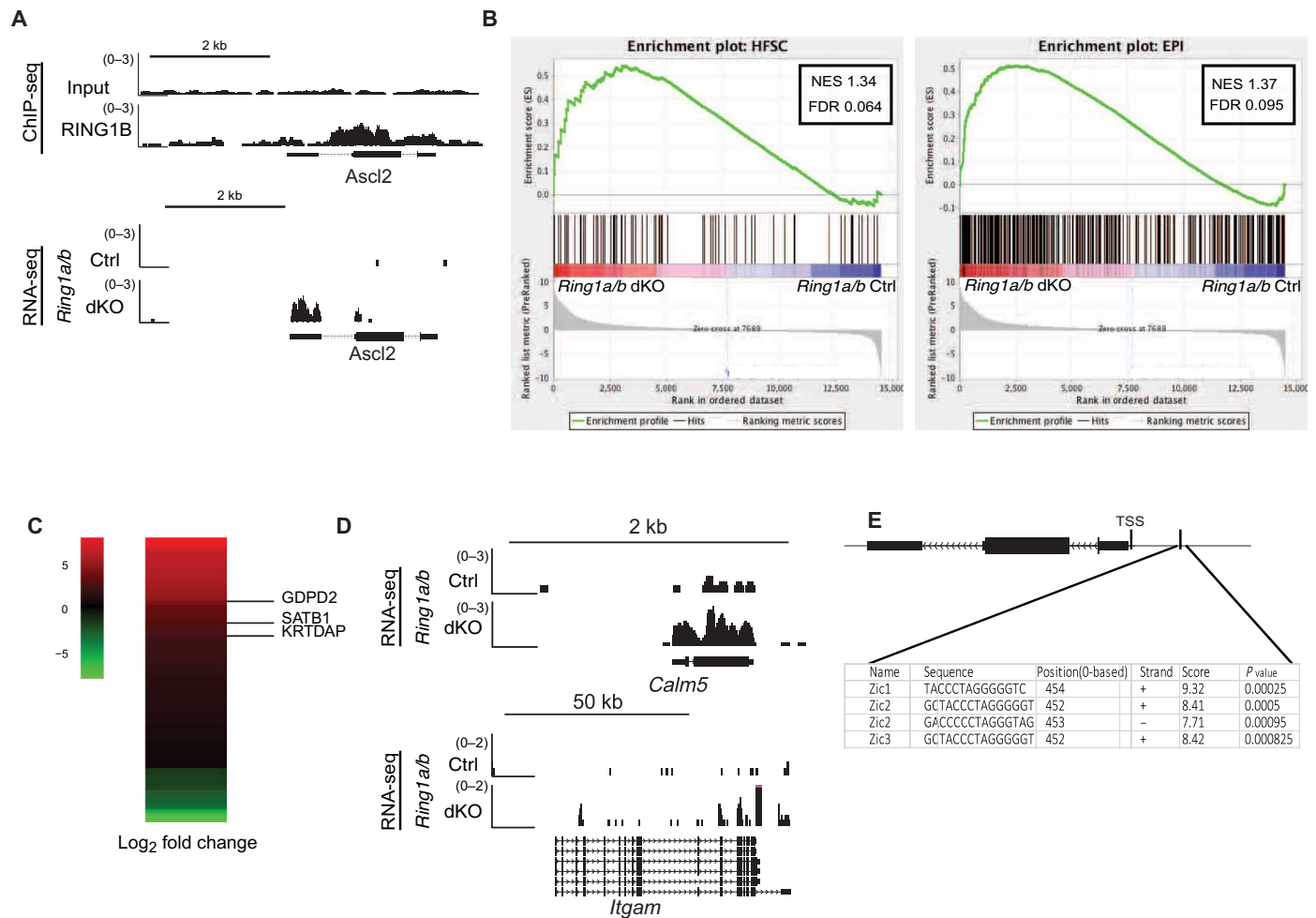
Fig. 5. PRC1 activity is required to maintained repressed the epidermal-specific transcriptional program in HFSCs. (**A**) RING1B occupancy at ASCL2 locus and transcriptional activation of ASCL2 in *Ring1a/b⁻/⁻*. (**B**) GSEAs performed on *Ring1a/b⁻/⁻* HFSCs using signatures specific for 14 major skin and HF cell populations (*31*). FDR, false discovery rate; NES, normalized enriched stone; EPI, epidermis. (**C**) Heatmap representing epidermal-specific genes differentially regulated in *Ring1a/b⁻/⁻* HFSCs (log₂ fold change). (**D**) Genomic snapshots of RNA-seq for *Calm5* and *Itgam* genes that are involved in epidermal differentiation. Chr13, chromosome 13. (**E**) Motif enrichment analyses on *Ascl2* promoter performed using LASAGNA-search 2.0 (*32*).

distribution has also been reported in murine ESCs, where H2AK119Ub1 and PRC2 co-occupy genes bound by CBX7/RING1B and are largely excluded by those regions exclusively bound by RYBP/RING1B (*33*). Note that, similar to ESCs, PRC1 localized on both repressed (canonical PcG targets) and active genes in both ISCs and HFSCs. This latter observation is in line with another recent report demonstrating a pivotal role of PRC1 during skin development (*11*). However, despite the fact that RYBP-containing PRC1 localizes to active promoters in both ISCs and HFSCs, very few of those active PRC1 targets score among the down-regulated genes, suggesting a marginal role of noncanonical complexes in preserving the expression of these target genes. This further restricts the specific phenotypes firstly described in ISCs and now documented in HFSCs to a more canonical PRC1 repressive activity. Our data demonstrate that several PcG direct targets became derepressed upon PRC1 loss of function and several of these targets can be directly linked to the observed phenotypic convergence. However, in HFSCs and ISCs, not all the PRC1 bound targets became activated upon RING1A/B loss. This suggests that, despite the idea that a general PRC1 role in maintaining repres-

sion of non–lineage-specific genes is, to some extent, conserved in cells of different developmental origin and tissues (i.e., HFSC, ESCs, and ISC), the transcriptional program triggered by its loss of function remains cell type dependent. This is likely due to the repertoire of available TFs in any given cell. Accordingly, among the different derepressed genes in *Ring1a/b* dKO HFSC, we found ASCL2, a DNA binding TF sufficient and required for epidermal differentiation (*30*). Further analysis of the transcriptome of PRC1-deficient HFSCs confirmed the activation of an ectopic, epidermal-specific, transcriptional program that could likely contribute for the observed phenotype.

Together, our data ultimately support the existence of a general role played by PRC1 to maintain adult stem cell identity that converge into a common phenotype with distinct cell type–specific mechanisms. This observation is of crucial importance not only to understand the role of Polycomb complexes in shaping adult tissues but also in different pathological settings, such as cancer, in which PcG is directly involved. The requirement of PcG during tumor development and progression, where a high level of cell heterogeneity can be observed, has been extensively reported, and several PcG

inhibitors entered clinical trials (*1*, *34*). In this context, the efficacy (i.e., the consequences) of PcG inhibition could be cell type specific, as we describe for adult stem cells, and possibly dependent on the integrity of the signaling pathways and on the TF repertoire of the different cells.

MATERIALS AND METHODS

Mouse models
Lgr5-specific conditional knockout mice were generated by crossing Ring1A$^{-/-}$ Ring1B$^{fl/fl}$ (*35*), with LGR5-eGFP-IRES-CreERT2 mice (*36*). These mice were crossed with Rosa26lox-stop-lox LacZ transgenic mice for in vivo lineage tracing (*37*). Genotyping was confirmed by polymerase chain reaction (PCR) of tail skin DNA. Cre-dependent recombination was induced performing three intraperitoneal injections of tamoxifen (Sigma-Aldrich) at 75 mg/kg.

Mice were maintained accordingly to the guidelines set out in Commission Recommendation 2007/526/EC, 18 June 2007, on guidelines for the accommodation and care of animals used for experimental and other scientific purposes. All experiments were performed in accordance with the Italian Laws (D.L.vo 116/92 and following additions), which enforces EU Directive 86/609 (Council Directive 86/609/EEC of 24 November 1986 on the approximation of laws, regulations, and administrative provisions of the member states regarding the protection of animals used for experimental and other scientific purposes).

HF purification
LGR5$^+$ cells were purified from back skin of treated mice at different time points. Subcutaneous fat and the blood vessels were removed, and the skin was digested using collagenase (2.5 mg/ml) in Dulbecco's modified Eagle's medium (DMEM) for 45 min. HFs were scraped off and incubated for 10 min at 37°C with 2.5% trypsin in phosphate-buffered saline (PBS) and deoxyribonuclease 1 (DNase1; 1600 U/ml). Fetal bovine serum was added to neutralize trypsin. Cells were washed with PBS and filtered with 70-μm cell strainer.

Flow cytometry and FACS
Single-cell suspension were washed and resuspended in sorting medium [DMEM; 1:100 penicillin and streptomicin (17-602F, Lonza), 1:100 L-glutamine (17-605E, Lonza), Hepes, 2 mM EDTA, DNase1 (800 U/ml), and 10 uM Y27632 (Selleck Chemicals)]. Single GFP$^+$ cells were FACS-sorted using either FACSMelody or FACSJazz cell sorters (BD Biosciences). Living cells were discriminated by propidium iodide exclusion staining.

Immunofluorescence
Back skin was harvested at the described time points, fixed with 4% paraformaldehyde (PFA) for 3 hours at 4°C, and cryopreserved in 30% sucrose overnight, followed by O.C.T. embedding (Tissue-TEK 4583). Embedded tissues were cut at 7 μm in thickness. Sections were washed in tris-buffered saline–0.1% Tween 20 (TBS-T) and blocked with 5% donkey serum at room temperature for 1 hour. Section were incubated with anti-H2AK119Ub (D27C4, Cell Signaling Technology) overnight at 4°C, washed in TBS-T, incubated for 1 hour at room temperature with secondary antibody [715-165-147, Cy3 AffiniPure Donkey Anti-Rabbit IgG (H+L), Jackson ImmunoResearch] and 4′,6-diamidino-2-phenylindole dihydrochloride (32670, Sigma-Aldrich), and mounted with Mowiol 4-88 (81381, Sigma-Aldrich). Images were taken with Leica Sp8 confocal microscope.

Proximity ligation assay
Anagen-induced sorted LGR5 HFSCs were spotted in Cell-Tak (Corning)–coated coverslip, and PLA was performed using Sigma-Aldrich Duolink In Situ Orange Starter Kit Mouse/Rabbit following the manufacturer's instruction protocol. Anti-RING1B antibody (homemade), anti-RYBP (AB3637, Millipore), and anti-BMI1 (homemade) primary antibodies were used.

Histology and lineage tracing
Freshly obtained back skin samples were collected at the indicated time point and were immediately prefixed for 30 min at room temperature in PBS containing 0.2% gluteraldehyde, 0.02% NP-40, and 2% PFA. Samples were washed three times for 10 min each with PBS and incubated for 30 min with the equilibration buffer (2 mM MgCl$_2$, 0.02 NP-40, and 0.1% sodium deoxycholate in PBS). Samples were stained overnight at room temperature using 5 mM K$_3$Fe(CN)$_6$, 5 mM K$_4$Fe(CN)$_6$, and X-Gal (1 mg/ml) in equilibration buffer. Stained skin were washed abundantly with PBS at room temperature and then fixed overnight in 4% PFA in PBS before paraffin embedding. Five-micrometer sections were obtained, rehydrated, and nuclei-counterstained with Nuclear Fast Red solution for 10 min at room temperature. For histological analysis, freshly isolated back skin samples were fixed in 4% formaldehyde overnight, paraffin-embedded, and stained with hematoxylin and eosin Y. Images were acquired using Olympus BX51 or Leica DM6 widefield microscope.

RNA sequencing
FACS-sorted cells were collected in 0.5-ml tubes and processed directly following Smart-seq2 protocol (*38*) with minor modifications. Briefly, 3000 cells per sample were collected directly and lysed in 2 μl of lysis buffer [0.2% Triton X-100 and ribonuclease inhibitor (4 U/μl)]. One microliter of 10 μM oligo-dT30Vn and 1 μl of 10 mM deoxynucleotide triphosphate were added, and the samples were incubated for 3 min at 72°C. Reverse transcriptase step was performed using SuperScript III reverse transcriptase enzyme (Invitrogen). Preamplification of the obtained complementary DNA (cDNA) was performed using KAPA Taq HotStart enzyme with High-Fidelity Buffer. Preamplified cDNA was purified using AMPure beads (Agencourt AMPure XP, Beckman Coulter), and the quality was checked using Bioanalyzer (Agilent). Two nanograms of cDNA was tagmented with 100 ng of homemade Tn5 enzyme and further amplified using KAPA HiFi HotStart Kit. Tagmented, amplified DNA was sequenced using Illumina HiSeq2000.

ChIP sequencing
LGR5$^+$ HFSCs were purified as previously described from anagen-synchronized HFs of Ring1a/b$^{+/+}$ mice and were extracted following the protocol previously described. A total of 2.5 million cells were used for ChIP-seq as previously described (*9*). Sonicated chromatin was incubated with 10 μg of rabbit anti-RING1B antibody (homemade), anti-H2AK119Ub1 (8240, Cell Signaling Technology), anti-RYBP (AB3637, Millipore), and anti-CBX8 (*39*) overnight, and the immunocomplexes recovered using protein A–conjugated magnetic beads (Dynabeads, Life Technologies). Purified chromatin was decross-linked overnight in 0.1 M NaHCO$_3$ and 1% SDS. Decross-linked DNA was purified. ISC-specific H3K4me3 ChIP-seq profile was obtained as previously described (*9*) using 5 μg of anti-H3K4Me3 antibody (catalog no. 39159, Active Motif).

RNA-seq analysis

Reads were aligned to the mouse reference genome mm9 using TopHat v2.1.1 (*40*) with parameters *--no-coverage-search* and *--library-type fr-unstranded*. PCR duplicates were removed using Picard (http://broadinstitute.github.io/picard/). Gene counts were calculated using HTSeq-count v0.8.0 (*41*) with parameters *--stranded=no --mode= intersection-nonempty* using RefSeq mm9 annotation downloaded from the University of California, Santa Cruz. Differential expression analyses were performed using the R package DESeq2 v1.20 (*42*) using default parameters. Genes with an absolute $\log_2$ fold change of 1 and false discovery rate of <0.1 were considered as differentially expressed. Gene enrichment analysis on down- and up-regulated genes was performed using DAVID 6.8 (*43*). A preranked GSEA (*44*) was performed using gene lists (Signature Gene Lists) from multiple skin cell populations obtained from (*31*). The analysis was performed using default parameters (weighted as enrichment statistic) and ranking the input gene list using $\log_2$ fold-change data obtained from DESeq2.

To assess the expression of differentially expressed genes in Ring1A/ B$^{-/-}$ versus wild-type HFSC in other mouse tissues, we used public RNA-seq data (bam files) deposited by ENCODE at (http://hgdownload. soe.ucsc.edu/goldenPath/mm9/encodeDCC/wgEncodeLicrRnaSeq/). Bam files were processed with the pipeline described previously, and RPKM (Read Per Kilobase of Milion Mapped Reads) data were normalized with the function normalize.quantiles() from the R package preprocessCore (https://github.com/bmbolstad/preprocessCore).

ChIP-seq analysis

Reads were aligned to the mouse reference genome mm9 using Bowtie v1.2.2 (*45*) with default parameters and not allowing multimapping (-m1). PCR duplicates were removed using Picard (http://broadinstitute.github.io/picard/). Peaks were called using MACS2 v2.1.1 (*46*) with parameters *-g mm --nomodel -p 1e-10 –B*. Genomic peak annotation was performed using the R package ChIPpeakAnno v3.15 (*47*), considering the promoter region of ±2.5 kb around the TSS (Transcription Start Site). Overlaps of ChIP-seq targets were performed as following: Genes with peaks in their promoter regions (±2.5 kb around TSS) were considered as targets. Then, the overlap between target gene lists was performed using the R package VennDiagram v1.6.20 (*48*).

For heatmap representation of ChIP-seq signal, bigwig files, with input signal subtracted, were generated using the function bamCompare from deepTools 2.0 (*49*) with parameters *--ratio subtract –bs 30 --extendReads 200*. To normalize for differences in sample library size, a scaling factor for each sample was calculated as (1/total mapped reads) × 1 million and applied during bigwig file generation with the parameter *–scaleFactors* from bamCompare.

Ring1b ChIP-seq targets were clustered in four groups according to their RPKM expression using the *dplyr* function *ntile()*. Tracks for H3K27me3 from ISC and HFSC were obtained from (*9*) and (*28*), respectively, and processed with the pipeline described previously.

SUPPLEMENTARY MATERIALS

Fig. S1. Mouse model of PRC1 activity abrogation.
Fig. S2. PRC1 loss severely affects anagen onset and progression.
Fig. S3. PRC1 loss has different transcriptional effects among tissues.
Fig. S4. Expression of core PRC1 subunits in HFSCs.
Fig. S5. Genomic distribution of PRC1 in ISCs resembles HFSCs.

REFERENCES AND NOTES

1. D. Pasini, L. Di Croce, Emerging roles for Polycomb proteins in cancer. *Curr. Opin. Genet. Dev.* **36**, 50–58 (2016).
2. B. Vogelstein, N. Papadopoulos, V. E. Velculescu, S. Zhou, L. A. Diaz Jr., K. W. Kinzler, Cancer genome landscapes. *Science* **339**, 1546–1558 (2013).
3. L. Di Croce, K. Helin, Transcriptional regulation by Polycomb group proteins. *Nat. Struct. Mol. Biol.* **20**, 1147–1155 (2013).
4. S. Aranda, G. Mas, L. Di Croce, Regulation of gene transcription by Polycomb proteins. *Sci. Adv.* **1**, e1500737 (2015).
5. A. Scelfo, A. Piunti, D. Pasini, The controversial role of the Polycomb group proteins in transcription and cancer: How much do we not understand Polycomb proteins? *FEBS J.* **282**, 1703–1722 (2015).
6. Z. Gao, J. Zhang, R. Bonasio, F. Strino, A. Sawai, F. Parisi, Y. Kluger, D. Reinberg, PCGF homologs, CBX proteins, and RYBP define functionally distinct PRC1 family complexes. *Mol. Cell* **45**, 344–356 (2012).
7. E. S. Bardot, V. J. Valdes, J. Zhang, C. N. Perdigoto, S. Nicolis, S. A. Hearn, J. M. Silva, E. Ezhkova, Polycomb subunits Ezh1 and Ezh2 regulate the Merkel cell differentiation program in skin stem cells. *EMBO J.* **32**, 1990–2000 (2013).
8. F. Chiacchiera, D. Pasini, Control of adult intestinal identity by the Polycomb repressive machinery. *Cell Cycle* **16**, 243–244 (2017).
9. F. Chiacchiera, A. Rossi, S. Jammula, A. Piunti, A. Scelfo, P. Ordóñez-Morán, J. Huelsken, H. Koseki, D. Pasini, Polycomb complex PRC1 preserves intestinal stem cell identity by sustaining Wnt/β-catenin transcriptional activity. *Cell Stem Cell* **18**, 91–103 (2016).
10. F. Chiacchiera, A. Rossi, S. Jammula, M. Zanotti, D. Pasini, PRC2 preserves intestinal progenitors and restricts secretory lineage commitment. *EMBO J.* **35**, 2301–2314 (2016).
11. I. Cohen, D. Zhao, C. Bar, V. J. Valdes, K. L. Dauber-Decker, M. B. Nguyen, M. Nakayama, M. Rendl, W. A. Bickmore, H. Koseki, D. Zheng, E. Ezhkova, PRC1 fine-tunes gene repression and activation to safeguard skin development and stem cell specification. *Cell Stem Cell* **22**, 726–739.e7 (2018).
12. K. L. Dauber, C. N. Perdigoto, V. J. Valdes, F. J. Santoriello, I. Cohen, E. Ezhkova, Dissecting the roles of Polycomb repressive complex 2 subunits in the control of skin development. *J. Invest. Dermatol.* **136**, 1647–1655 (2016).
13. E. Ezhkova, W.-H. Lien, N. Stokes, H. A. Pasolli, J. M. Silva, E. Fuchs, EZH1 and EZH2 cogovern histone H3K27 trimethylation and are essential for hair follicle homeostasis and wound repair. *Genes Dev.* **25**, 485–498 (2011).
14. M. Vidal, K. Starowicz, Polycomb complexes PRC1 and their function in hematopoiesis. *Exp. Hematol.* **48**, 12–31 (2017).
15. N. Barker, S. Bartfeld, H. Clevers, Tissue-resident adult stem cell populations of rapidly self-renewing organs. *Cell Stem Cell* **7**, 656–670 (2010).
16. E. Fuchs, Epithelial skin biology: Three decades of developmental biology, a hundred questions answered and a thousand new ones to address. *Curr. Top. Dev. Biol.* **116**, 357–374 (2016).
17. A. Haegebarth, H. Clevers, Wnt signaling, Lgr5, and stem cells in the intestine and skin. *Am. J. Pathol.* **174**, 715–721 (2009).
18. V. Jaks, N. Barker, M. Kasper, J. H. van Es, H. J. Snippert, H. Clevers, R. Toftgård, Lgr5 marks cycling, yet long-lived, hair follicle stem cells. *Nat. Genet.* **40**, 1291–1299 (2008).
19. R. Paus, S. Müller-Röver, C. van der Veen, M. Maurer, S. Eichmüller, G. Ling, U. Hofmann, K. Foitzik, L. Mecklenburg, B. Handjiski, A comprehensive guide for the recognition and classification of distinct stages of hair follicle morphogenesis. *J. Invest. Dermatol.* **113**, 523–532 (1999).
20. R. C. Adam, H. Yang, Y. Ge, W.-H. Lien, P. Wang, Y. Zhao, L. Polak, J. Levorse, S. C. Baksh, D. Zheng, E. Fuchs, Temporal layering of signaling effectors drives chromatin remodeling during hair follicle stem cell lineage progression. *Cell Stem Cell* **22**, 398–413.e7 (2018).
21. V. Greco, T. Chen, M. Rendl, M. Schober, H. A. Pasolli, N. Stokes, J. dela Cruz-Racelis, E. Fuchs, A two-step mechanism for stem cell activation during hair regeneration. *Cell Stem Cell* **4**, 155–169 (2009).
22. J. D. Hoeck, B. Biehs, A. V. Kurtova, N. M. Kljavin, F. de Sousa e Melo, B. Alicke, H. Koeppen, Z. Modrusan, R. Piskol, F. J. de Sauvage, Stem cell plasticity enables hair regeneration following *Lgr5*+ cell loss. *Nat. Cell Biol.* **19**, 666–676 (2017).
23. Y.-C. Hsu, L. Li, E. Fuchs, Transit-amplifying cells orchestrate stem cell activity and tissue regeneration. *Cell* **157**, 935–949 (2014).
24. H. Yang, R. C. Adam, Y. Ge, Z. L. Hua, E. Fuchs, Epithelial-mesenchymal micro-niches govern stem cell lineage choices. *Cell* **169**, 483–496.e13 (2017).
25. S. Müller-Röver, K. Foitzik, R. Paus, B. Handjiski, C. der Veen, S. Eichmüller, I. A. McKay, K. S. Stenn, A comprehensive guide for the accurate classification of murine hair follicles in distinct hair cycle stages. *J. Invest. Dermatol.* **117**, 3–15 (2001).
26. A. R. Foster, C. Nicu, M. R. Schneider, E. Hinde, R. Paus, Dermal white adipose tissue undergoes major morphological changes during the spontaneous and induced murine hair follicle cycling: A reappraisal. *Arch. Dermatol. Res.* **310**, 453–462 (2018).

27. B. St-Jacques, H. R. Dassule, I. Karavanova, V. A. Botchkarev, J. Li, P. S. Danielian, J. A. McMahon, P. M. Lewis, R. Paus, A. P. McMahon, Sonic hedgehog signaling is essential for hair development. *Curr. Biol.* **8**, 1058–1069 (1998).

28. W. H. Lien, X. Guo, L. Polak, L. N. Lawton, R. A. Young, D. Zheng, E. Fuchs, Genome-wide maps of histone modifications unwind in vivo chromatin states of the hair follicle lineage. *Cell Stem Cell* **9**, 219–232 (2011).

29. B. E. Bernstein, T. S. Mikkelsen, X. Xie, M. Kamal, D. J. Huebert, J. Cuff, B. Fry, A. Meissner, M. Wernig, K. Plath, R. Jaenisch, A. Wagschal, R. Feil, S. L. Schreiber, E. S. Lander, A bivalent chromatin structure marks key developmental genes in embryonic stem cells. *Cell* **125**, 315–326 (2006).

30. M. Moriyama, A.-D. Durham, H. Moriyama, K. Hasegawa, S.-I. Nishikawa, F. Radtke, M. Osawa, Multiple roles of Notch signaling in the regulation of epidermal development. *Dev. Cell* **14**, 594–604 (2008).

31. A. Rezza, Z. Wang, R. Sennett, W. Qiao, D. Wang, N. Heitman, K. W. Mok, C. Clavel, R. Yi, P. Zandstra, A. Ma'ayan, M. Rendl, Signaling networks among stem cell precursors, transit-amplifying progenitors, and their niche in developing hair follicles. *Cell Rep.* **14**, 3001–3018 (2016).

32. C. Lee, C.-H. Huang, LASAGNA-Search 2.0: Integrated transcription factor binding site search and visualization in a browser. *Bioinformatics* **30**, 1923–1925 (2014).

33. L. Morey, L. Aloia, L. Cozzuto, S. A. Benitah, L. Di Croce, RYBP and Cbx7 define specific biological functions of polycomb complexes in mouse embryonic stem cells. *Cell Rep.* **3**, 60–69 (2013).

34. H. Richly, L. Aloia, L. Di Croce, Roles of the Polycomb group proteins in stem cells and cancer. *Cell Death Dis.* **2**, e204 (2011).

35. M. de Napoles, J. E. Mermoud, R. Wakao, Y. A. Tang, M. Endoh, R. Appanah, T. B. Nesterova, J. Silva, A. P. Otte, M. Vidal, H. Koseki, N. Brockdorff, Polycomb group proteins Ring1A/B link ubiquitylation of histone H2A to heritable gene silencing and X inactivation. *Dev. Cell* **7**, 663–676 (2004).

36. N. Barker, J. H. van Es, J. Kuipers, P. Kujala, M. van den Born, M. Cozijnsen, A. Haegebarth, J. Korving, H. Begthel, P. J. Peters, H. Clevers, Identification of stem cells in small intestine and colon by marker gene *Lgr5*. *Nature* **449**, 1003–1007 (2007).

37. P. Soriano, Generalized *lacZ* expression with the ROSA26 Cre reporter strain. *Nat. Genet.* **21**, 70–71 (1999).

38. S. Picelli, O. R. Faridani, Å. K. Björklund, G. Winberg, S. Sagasser, R. Sandberg, Full-length RNA-seq from single cells using Smart-seq2. *Nat. Protoc.* **9**, 171–181 (2014).

39. A. P. Bracken, N. Dietrich, D. Pasini, K. H. Hansen, K. Helin, Genome-wide mapping of Polycomb target genes unravels their roles in cell fate transitions. *Genes Dev.* **20**, 1123–1136 (2006).

40. C. Trapnell, L. Pachter, S. L. Salzberg, TopHat: Discovering splice junctions with RNA-seq. *Bioinformatics* **25**, 1105–1111 (2009).

41. S. Anders, P. T. Pyl, W. Huber, HTSeq—A Python framework to work with high-throughput sequencing data. *Bioinformatics* **31**, 166–169 (2015).

42. M. I. Love, W. Huber, S. Anders, Moderated estimation of fold change and dispersion for RNA-seq data with DESeq2. *Genome Biol.* **15**, 550 (2014).

43. D. W. Huang, B. T. Sherman, R. A. Lempicki, Systematic and integrative analysis of large gene lists using DAVID bioinformatics resources. *Nat. Protoc.* **4**, 44–57 (2009).

44. A. Subramanian, P. Tamayo, V. K. Mootha, S. Mukherjee, B. L. Ebert, M. A. Gillette, A. Paulovich, S. L. Pomeroy, T. R. Golub, E. S. Lander, J. P. Mesirov, Gene set enrichment analysis: A knowledge-based approach for interpreting genome-wide expression profiles. *Proc. Natl. Acad. Sci. U.S.A.* **102**, 15545–15550 (2005).

45. B. Langmead, C. Trapnell, M. Pop, S. L. Salzberg, Ultrafast and memory-efficient alignment of short DNA sequences to the human genome. *Genome Biol.* **10**, R25 (2009).

46. Y. Zhang, T. Liu, C. A. Meyer, J. Eeckhoute, D. S. Johnson, B. E. Bernstein, C. Nusbaum, R. M. Myers, M. Brown, W. Li, X. S. Liu, Model-based Analysis of ChIP-Seq (MACS). *Genome Biol.* **9**, R137 (2008).

47. L. J. Zhu, C. Gazin, N. D. Lawson, H. Pagès, S. M. Lin, D. S. Lapointe, M. R. Green, ChIPpeakAnno: A Bioconductor package to annotate ChIP-seq and ChIP-chip data. *BMC Bioinf.* **11**, 237 (2010).

48. H. Chen, P. C. Boutros, VennDiagram: A package for the generation of highly-customizable Venn and Euler diagrams in R. *BMC Bioinf.* **12**, 35 (2011).

49. F. Ramírez, D. P. Ryan, B. Grüning, V. Bhardwaj, F. Kilpert, A. S. Richter, S. Heyne, F. Dündar, T. Manke, deepTools2: A next generation web server for deep-sequencing data analysis. *Nucleic Acids Res.* **44**, W160–W165 (2016).

Citation: S. Pivetti, D. Fernandez-Perez, A. D'Ambrosio, C. M. Barbieri, D. Manganaro, A. Rossi, L. Barnabei, M. Zanotti, A. Scelfo, F. Chiacchiera, D. Pasini, Loss of PRC1 activity in different stem cell compartments activates a common transcriptional program with cell type–dependent outcomes. *Sci. Adv.* **5**, eaav1594 (2019).

Science Advances

Loss of PRC1 activity in different stem cell compartments activates a common transcriptional program with cell type–dependent outcomes

Silvia Pivetti, Daniel Fernandez-Perez, Alessandro D'Ambrosio, Caterina Maria Barbieri, Daria Manganaro, Alessandra Rossi, Laura Barnabei, Marika Zanotti, Andrea Scelfo, Fulvio Chiacchiera and Diego Pasini

ARTICLE TOOLS	http://advances.sciencemag.org/content/5/5/eaav1594
SUPPLEMENTARY MATERIALS	http://advances.sciencemag.org/content/suppl/2019/05/13/5.5.eaav1594.DC1
REFERENCES	This article cites 49 articles, 7 of which you can access for free http://advances.sciencemag.org/content/5/5/eaav1594#BIBL
PERMISSIONS	http://www.sciencemag.org/help/reprints-and-permissions

Use of this article is subject to the Terms of Service